



HAL
open science

MicroRNA miR-885-5p targets CDK2 and MCM5, activates p53 and inhibits proliferation and survival

Frank Westermann, Elena Afanasyeva, Pieter Mestdagh, Candy Kumps, Jo Vandesompele, Volker Ehemann, Jessika Theissen, Matthias Fischer, Marc Zapatka, Benedikt Brors, et al.

► To cite this version:

Frank Westermann, Elena Afanasyeva, Pieter Mestdagh, Candy Kumps, Jo Vandesompele, et al.. MicroRNA miR-885-5p targets CDK2 and MCM5, activates p53 and inhibits proliferation and survival. Cell Death and Differentiation, 2011, 10.1038/cdd.2010.164 . hal-00608714

HAL Id: hal-00608714

<https://hal.science/hal-00608714>

Submitted on 14 Jul 2011

HAL is a multi-disciplinary open access archive for the deposit and dissemination of scientific research documents, whether they are published or not. The documents may come from teaching and research institutions in France or abroad, or from public or private research centers.

L'archive ouverte pluridisciplinaire **HAL**, est destinée au dépôt et à la diffusion de documents scientifiques de niveau recherche, publiés ou non, émanant des établissements d'enseignement et de recherche français ou étrangers, des laboratoires publics ou privés.

MicroRNA miR-885-5p targets CDK2 and MCM5, activates p53 and inhibits proliferation and survival

Elena A. Afanasyeva¹, Pieter Mestdagh³, Candy Kumps³, Jo Vandesompele³, Volker Ehemann²,
Jessica Theissen⁴, Matthias Fischer⁴, Marc Zapatka⁵, Benedikt Brors⁵, Larissa Savelyeva¹, Vitaliya
Sagulenko¹, Frank Speleman³, Manfred Schwab¹, Frank Westermann^{1*}

¹Department of Tumor Genetics, B030, German Cancer Research Center, Im Neuenheimer Feld 280,
D-69120 Heidelberg, Germany

²Department of Cytometry, Institute of Pathology, Im Neuenheimer Feld 220, D-69120 Heidelberg,
Germany

³Center for Medical Genetics, Ghent University Hospital, De Pintelaan 185, B-9000 Ghent, Belgium

⁴Department of Pediatric Oncology and Hematology, University Children's Hospital, and Center for
Molecular Medicine Cologne (CMMC), Kerpener Strasse 62, 50924 Cologne, Germany

⁵Theoretical Bioinformatics B080, German Cancer Research Center (DKFZ), Im Neuenheimer Feld
580, Heidelberg, Germany

*To whom correspondences should be addressed (f.westermann@dkfz-heidelberg.de)

Tel. +49 6221 423275

Fax: +49 6221 423277

Running title: *miR-885-5p* activates p53 pathway

Abstract

Several miRNA loci are found within genomic regions frequently deleted in primary neuroblastoma, including *miR-885-5p* at 3p25.3. Here we demonstrate that *miR-885-5p* is downregulated upon loss of 3p25.3 region in neuroblastoma. Experimentally enforced miR-885-5p expression in neuroblastoma cell lines inhibits proliferation triggering cell cycle arrest, senescence and/or apoptosis. miR-885-5p leads to accumulation of p53 protein and activates the p53 pathway, resulting in upregulation of p53 targets. Enforced miR-885-5p expression consistently leads to downregulation of *CDK2* and *MCM5*. Both genes are targeted by miR-885-5p via predicted binding sites within the 3'UTRs of *CDK2* and *MCM5*. Transcript profiling after miR-885-5p introduction in neuroblastoma cells reveals alterations in expression of multiple genes, including several p53 target genes and a number of factors involved in p53 pathway activity. Taken together, these data provide evidence that miR-885-5p has a tumor suppressive role in neuroblastoma interfering with cell cycle progression and cell survival.

Key words: 3p25.3/miRNA/p53 stabilization/senescence

Introduction

MicroRNAs (miRNAs) are non-coding short (18-24nt) RNAs, which control gene expression at a posttranscriptional level via inhibiting translation or triggering degradation of multiple target mRNAs. They are considered as vitally important regulators of proliferation, differentiation and apoptosis. Upregulated and downregulated miRNAs have been found in different malignancies, thus implicating that miRNAs act as oncogenes or tumor suppressors¹. Moreover, an increasing body of evidence for miRNA involvement in tumorigenesis has prompted researchers to revisit cancer-associated genomic regions to search for miRNA loci². For example, *miR-15* and *miR-16*, mapping to a deletion region at 13q14, are downregulated in B-cell chronic lymphocytic leukaemia. Both miR-15 and miR-16 negatively regulate BCL2 and act as positive regulators of apoptosis, which could explain their frequent inactivation in leukaemia³. Later, *miR-34a* at 1p36 emerged as a tumor suppressor gene (TSG). Several independent studies demonstrated the anti-proliferative and proapoptotic potential of miR-34a^{4, 5}. The potential is great for the involvement of many other, as yet unreported, miRNAs in cancer pathogenesis.

Neural crest-derived neuroblastoma, one of the most common solid tumors in children, is frequently characterized as an “enigmatic neoplasm”. Indeed, neuroblastoma has the highest rate of spontaneous regression of all human malignancies. On the other hand, approximately 40% of neuroblastomas rapidly progress despite multimodal treatment regimes^{6, 7}. Another interesting characteristic of neuroblastoma is the rarity of *TP53* mutations; neuroblastoma retain very often functional p53. These facts suggest that the inhibitors of p53 pathway or a loss of p53 pathway positive regulators may be involved in neutralizing of p53 activity^{8, 9}. Neuroblastomas with poor outcome are subdivided into at least two biologically distinct groups. One group includes neuroblastomas harboring amplification of the *MYCN* oncogene, and a second group lacks amplified *MYCN*. It is known that this second group also frequently harbors segmental 3p deletions¹⁰, which implies that neuroblastoma suppressive transcripts are encoded from this region. Several efforts have been made to map and refine the critical

region for 3p loss in neuroblastoma. Currently, a consensus region of loss is assigned to 3p25-26.2, which includes the *VHL* gene. Low *VHL* mRNA expression does correlate with poor prognosis, however, functional analyses could not reveal differences in pVHL protein expression nor pVHL pathway impairment¹¹. To date, the identity of neuroblastoma-relevant tumor suppressor genes (TSGs) at 3p25-26.2 is unknown. In a previous study we detected several known and novel miRNA loci located within regions of neuroblastoma-relevant chromosomal aberrations¹². We focus here on *miR-885-5p*, the only *miRNA* gene mapping to 3p25.3. We show that miR-885-5p is able to interfere with cell proliferation and survival, promoting cellular senescence and apoptosis. Furthermore, we demonstrate that miR-885-5p downregulates CDK2 and MCM5, activates p53 and provide evidence that CDK2 and MCM5 are direct miR-885-5p targets. Our results suggest a tumor suppressive role for miR-885-5p in neuroblastoma.

Results

Low miR-885-5p expression in primary neuroblastomas with segmental 3p loss

In our previous work characterizing the neuroblastoma miRNA transcriptome we cloned miR-885-5p (MYCN_{SC}_5_281) from a favorable tumor. *miR-885-5p* is a nonconserved *miRNA* that has no homologues in mouse and rat genomes (Supplementary Figure S1a). To evaluate rearrangements of the region encompassing *miR-885-5p* in primary neuroblastomas, we used array-based comparative genomic hybridization (aCGH) to analyze 193 neuroblastomas with different clinical and biological characteristics. The 3p25.3 region encompassing *miR-885-5p* was heterozygously deleted in the context of a segmental chromosomal 3p loss in 14% (n=27) of tumours (Figure 1a). Among the 3p deleted tumors, most were stage 4 (n=17). These data are consistent with previous reports on 3p25.3 status in

neuroblastoma¹⁰. We profiled the expression of *miR-885-5p* by reverse transcription quantitative PCR (RT-qPCR) in 60 primary neuroblastomas. As a comparison, we profiled *miR-331-3p*, a miRNA that might be repressed by *MYCN* according to our previous data¹² and that might also have tumor suppressive functions. Assuming equal Cq-values for similar expression levels, expression of *miR-885-5p* appears to be lower than of *miR-331-3p* in neuroblastoma tumours (Figure 1b). No significant difference in *miR-885-5p* expression was detected between neuroblastomas with and without *MYCN* amplification, whereas *miR-331-3p* expression was lower in *MYCN*-amplified neuroblastomas ($P<0.001$, Figure 1b). Intriguingly, *miR-885-5p* expression was lower in aggressive tumors with segmental 3p deletions, as compared to those with intact 3p and favourable prognosis ($P=0.02$, Figure 1b). Expression of *miR-885-5p* and *miR-331-3p* was measured in nine neuroblastoma cell lines using RT-qPCR and northern blotting. Both *MYCN*-nonamplified cell lines as well as *MYCN*-amplified cell lines were assessed (Figure 1c). Expression of the precursor and mature *miR-885-5p* was low in all cell lines analyzed and lacked correlation with 3p25 status, while expression of precursor and mature form of *miR-331-3p* was higher and did not vary significantly (Figure 1d; Supplementary Figure S1b). In neuroblastoma cell lines, expression of *miR-885-5p* lacked correlation with 3p25 status, suggesting that also other miR-885-5p inactivating lesions in neuroblastoma cells exist.

Our data support a tumor suppressive role of miR-885-5p at least in a group of neuroblastomas with intact 3p25.3. miR-331-3p data are less supportive, however, we included miR-331-3p further in our study as a positive control to monitor the specificity of miR-885-5p-mediated effects.

miR-885-5p inhibits neuroblastoma proliferation and survival

For functional analysis of miR-885-5p in neuroblastoma cells, we introduced miR-885-5p mimics into KELLY, IMR32, SK-N-BE(2)c, SH-EP and HDN33 cell lines. SH-EP, KELLY and IMR32 cell lines

have wild-type *TP53*, while p53 in SK-N-BE(2)c lacks transcription factor activity due to mutation in the DNA-binding domain¹³. The p53 pathway may not be intact in HDN33 based on the presence of centrosome amplification, multinuclear cells^{14, 15} and heterozygous mutation leading to an amino acid change at codon 15 (Ser to Cys) (Supplementary Figure S2). Cell proliferation was assessed in cells transiently transfected with either the miR-885-5p mimic, the miR-331-3p mimic or a nontargeting control miRNA using Alamar Blue assay. Enforced miR-885-5p expression reduced proliferation capacity in all cell lines analyzed, whereas transfection of miR-331-3p only inhibited proliferation in the HDN33 and SK-N-BE(2)c cell lines (Figure 2a). SH-EP, KELLY, IMR32 and SK-N-BE(2)c cells were also less capable of anchorage-independent growth in soft agar after enforced miR-885-5p expression (Figure 2b). Importantly, suppression of anchorage-independent growth after miR-885-5p introduction was more pronounced in cell lines with wild-type *TP53* (KELLY, IMR32 and SH-EP) than in SK-N-BE(2)c cells with mutant *TP53*. Enforced miR-331-3p expression only reduced colony growth of SK-N-BE(2)c cells in soft agar. We also tested whether proliferation inhibition by miR-885-5p was associated with senescence. Senescence-associated acidic β -galactosidase (SA- β -Gal) activity was detected in miR-885-5p-transfected *MYCN* nonamplified HDN33 and SH-EP cells (Figure 2a, insert), but not in *MYCN* amplified KELLY, IMR32, and SK-N-BE(2)c cells (data not shown).

Cell cycle profiles were also analyzed after enforced expression of either miR-885-5p or miR-331-3p using flow cytometry (FACS). Accumulation in G₁/G₀ after miR-885-5p transfection was observed in cell lines with wild-type *TP53* (KELLY, IMR32 and SH-EP) (Figure 2c), whereas enforced miR-885-5p expression in SK-N-BE(2)c and HDN33 resulted in accumulation of cells in S and G₂/M phase, respectively. In contrast, enforced miR-331-3p expression did not lead to pronounced cell cycle changes (> \pm 3%) in IMR32, KELLY and SH-EP cells. Enforced miR-331-3p expression in HDN33 resulted in G₁/G₀ and in SK-N-BE(2)c in G₂/M accumulation. To ascertain whether the observed cell cycle changes were accompanied by cell death, we analyzed the sub-G₁ fraction. Enforced miR-885-5p expression slightly increased the sub-G₁ fraction of SH-EP and IMR32 and moderately in SK-N-

BE(2)c and HDN33 cells, whereas the sub-G1 fraction after miR-331-3p transfection was only increased in SK-N-BE(2)c cells (Figure 2d). The amount of Annexin V-positive cells was elevated after miR-885-5p treatment in HDN33 and SK-N-BE(2)c but not in IMR32, KELLY and SH-EP (Figure 2d, insert; data not shown).

Taken together, these data suggest that miR-885-5p mediated inhibition of neuroblastoma proliferation is preferentially via G_0/G_1 arrest in *TP53* wild-type cells (IMR32, KELLY and SH-EP) and by apoptotic cell death in neuroblastoma cells with disabled p53 pathway (SK-N-BE(2)c and HDN33).

miR-885-5p induces p53 and downregulates CDK2 and MCM5

To further analyze the role of miR-885-5p on p53 regulation and function, we measured protein levels of p53 and its downstream targets after enforced miR-885-5p expression. We observed a marked p53 induction in KELLY and IMR32 cells, and a moderate p53 induction in SH-EP cells after miR-885-5p transfection (Figure 3a). Transfection of miR-885-5p also induced p53 in *TP53* mutant SK-N-BE(2)c cells. Enforced miR-885-5p expression resulted in elevated p21^{waf1} levels in KELLY, IMR32 and SH-EP cells; PUMA was elevated only in IMR32 cells. Enforced miR-885-5p expression did not alter p53 and p21^{waf1} protein expression in HDN33 cells or p21^{waf1} and PUMA protein expression in *TP53* mutant SK-N-BE(2)c cells, and miR-331-3p expression had no effect on p53, p21^{waf1} and PUMA protein levels in any of the cell lines analyzed. Expression of miR-885-5p downregulated E2F1 in SH-EP, IMR32, KELLY and HDN33 cells, while it had no effect on MYCN and p27 protein levels (Figure 3a, and data not shown). Caspase-3 activity was elevated in SK-N-BE(2)c and IMR32 after miR-885-5p introduction although the increases were less than two fold (Supplementary Figure S3). Western

blot analysis revealed reduction of procaspase-3 levels in all cell lines (Figure 3a) with no significant appearance of mature caspase-3 (data not shown). Taken together, the western blot data reveal that enforced miR-885-5p expression causes p53 and p21^{waf1} induction in *TP53* wild-type neuroblastoma, which is in line with the observed G₀/G₁ arrest after enforced expression of this miRNA.

Querying the miRNA databases at www.microrna.org¹⁶, TargetScan¹⁷ (www.targetscan.org) and searching for candidate 3'UTRs using the miRanda algorithm¹⁸ in the UTRResource 3'UTR database (<http://www.ba.itb.cnr.it/UTR/>) retrieved STAT3, CUL3, CDK2, MCM3, MCM5 and CDK6 as candidate miR-885-5p targets, and p21^{waf1} and E2F1 as candidate miR-331-3p targets. Cleavage of STAT3 and MCM3 by apoptosis-executing proteases has been reported, which could have interfered with our expression analysis of these proteins^{19,20}. We examined the protein expression of the candidate targets after miR-885-5p and miR-331-3p transfection. CDK2 and MCM5 protein levels decreased after miR-885-5p transfection in all tested cell lines, supporting both as direct miR-885-5p targets (Figure 3b). Enforced miR-331-3p expression reduced E2F1 levels in KELLY, IMR32 and SK-N-BE(2)c and reduced CDK2 expression in IMR32, although to a lesser extent than miR-885-5p. MCM3 cleavage was observed after miR-885-5p transfection of IMR32 and SK-N-BE(2)c cells, which prohibited estimation of direct targeting of MCM3 by miR-885-5p.

To test whether the observed effects of miR-885-5p depend on the manner of overexpressing miRNAs SH-EP and KELLY cell lines stably expressing either miR-885-5p or miR-331-3p were generated (Supplementary Figure S1c). The phenotype of miR-885-5p-SH-EP and miR-885-5p-KELLY cells was highly similar to that of SH-EP and KELLY cells transiently transfected with the miR-885-5p mimic. Most importantly, CDK2 and MCM5 were downregulated and p53 and p21^{waf1} were upregulated in only the miR-885-5p-SH-EP cells and miR-885-5p-KELLY cells (Supplementary Figure S4).

Accordingly, our data from *in silico* prediction and western blotting support the notion that CDK2 and MCM5 are targeted by miR-885-5p.

miR-885-5p directly targets the predicted binding sites in *CDK2* and *MCM5* 3'-UTRs.

To test whether miR-885-5p binding sites in the *CDK2* and *MCM5* 3'UTRs are directly regulated by miR-885-5p we performed luciferase reporter assays. Relative firefly luciferase activities of reporter plasmids containing *MCM5* or *CDK2* 3'-UTR binding sites were inhibited by 20-40% in miR-885-5p-SH-EP cells and premiR-885-5p-transfected SH-EP cells but not parental, vector- or miR-331-3p-SH-EP cells and control miRNA or miR-331-3p-transfected cells. Importantly, mutation of the *CDK2* and *MCM5* binding sites in the reporter constructs restored luciferase activity in miR-885-5p-SH-EP and premiR-885-5p-transfected cells (Figure 4).

These data show that miR-885-5p directly targets the predicted binding sites in the 3'UTRs of *CDK2* and *MCM5*.

CDK2 and MCM5 knockdown mimic miR-885-5p-induced phenotype

Previous studies showed that CDK2 and MCM5 are connected to the p53 pathway. MCM5 was identified as a negative regulator of p53-induced growth arrest²¹. Moreover, CDK2 inhibition led to p53 accumulation in *MYCN*-amplified neuroblastoma cells²². This suggests a link between phenotypic changes induced by miR-885-5p in neuroblastoma cells and suppression of CDK2 and MCM5. To test this possibility we introduced siRNAs targeting CDK2 and/or MCM5 into the given set of neuroblastoma cells lines and analyzed the phenotype with the same panel of assays used for the

characterization of the miR-885-5p-induced phenotype. CDK2 or MCM5 knockdown alone as well as the combined knockdown inhibited cell proliferation and anchorage-independent growth in all tested cell lines (Figure 5ab). Cell cycle analysis at day 3 after transfection of CDK2 or CDK2/MCM5 siRNAs revealed accumulation of cells in G₁/G₀ phase in most cell lines (SH-EP, KELLY, IMR32 and HDN33, Figure 5a). MCM5 knockdown alone showed an inconsistent cell cycle phenotype with G₁/G₀ arrest in SH-EP and KELLY and G₂/M arrest in the other cell lines. SK-N-BE(2)c cells failed to respond with a G₁/G₀ arrest after CDK2 and/or MCM5 knockdown, but consistently showed accumulation of cells in G₂/M phase. Most SA-β-Gal positive cells were found after the combined CDK2/MCM5 knockdown in SH-EP and HDN33 cells (Figure 5c), both of which also showed SA-β-Gal positive cells after miR-885-5p overexpression. In addition, an increase of sub-G₁ fraction and Annexin V positive cells were observed in HDN33 after CDK2 and/or MCM5 knockdown (Figure 5c), which were also observed after miR-885-5p overexpression in these cells. Neither CDK2 nor MCM5 inhibition led to significant increases in apoptotic cell death in SH-EP, KELLY, IMR32 and SK-N-BE(2)c.

We found p53 and p21^{waf1} upregulation after CDK2 knockdown in SH-EP, KELLY and IMR32 cells and PUMA upregulation after CDK2 knockdown in IMR32 cells (Figure 5d). CDK2 and/or MCM5 knockdown did not affect p53, p21^{waf1} and PUMA levels in HDN33 cells. Together, these data suggest that CDK2 and MCM5 inhibition is involved in miR-885-5p-mediated growth arrest and senescence in *TP53* wild-type neuroblastoma cells. Also, CDK2 and MCM5 inhibition can play a role in miR-885-5p-triggered apoptosis and senescence in *TP53* mutant HDN33 cells. However, although CDK2 and/or MCM5 knockdown in SK-N-BE(2)c shared p53 upregulation with miR-885-5p-transfected SK-N-BE(2)c, they did not undergo apoptosis, suggesting that targets other than CDK2 and MCM5 modify the SK-N-BE(2)c response to miR-885-5p.

miR-885-5p-induced growth arrest is p53 dependent in *TP53* wild-type neuroblastoma

To determine whether miR-885-5p-induced growth arrest is indeed p53-dependent in *TP53* wild-type neuroblastoma we sequentially transfected *TP53* wild-type SH-EP, KELLY and IMR32 cells with siRNA targeting p53 and miRNA mimics and assessed cell proliferation with Alamar Blue assay. While the treatment of control siRNA transfected cells with premiRs induced the same phenotype as premiR treatment alone, miR-885-5p failed to inhibit proliferation in p53 knockdown SH-EP, KELLY and IMR32 cells. In addition, p53-knockdown abolished miR-885-5p-induced G₁/G₀ arrest and inhibition of anchorage independent growth by miR-885-5p in these cells (Figure 6ab). Consistently, the levels of p21^{waf1} and PUMA remained unaffected in response to miR-885-5p and after p53 knockdown in these cells (Figure 6c).

To further validate that miR-885-5p regulates p53, CDK2 and MCM5 we thought to suppress endogenous miR-885-5p in neuroblastoma cells. According to our RT-qPCR and northern blot data (Figure 1d, Supplementary Figure S1) only IMR32 and SK-N-BE(2)c cells express significant levels of miR-885-5p. We did not observe growth upregulation upon antimiR-885-5p as determined by Alamar Blue assay (data not shown). However, a trend towards increased anchorage-independent growth was found in antimiR-885-5p transfected IMR32 and SK-N-BE(2)c cells. Importantly, p53, p21^{waf1} and PUMA levels were reduced in antimir-885-5p-transfected SK-N-BE(2)c and IMR32 (Figure 6d). Moreover, MCM5 was moderately induced in antimiR-885-5p-transfected SK-N-BE(2)c and CDK2 was induced in antimiR-885-5p-transfected SK-N-BE(2)c and IMR32 (Figure 6d). According to these data, antimiR-885-5p affects p53, p21^{waf1}, CDK2 and MCM5 protein levels altogether, which is consistent with the results from miRNA mimic transfections and strengthens the link between miR-

885-5p and p53/CDK2/MCM5.

miR-885-5p activates the p53 transcriptional program

In previous sections we provide evidence that miR-885-5p-mediated growth inhibition requires functional p53 in *TP53* wild-type neuroblastoma cells. To further characterize downstream effects of miR-885-5p expression in neuroblastoma cells with wild-type *TP53*, gene expression profiles 3 days after miR-885-5p mimic transfection in SH-EP and KELLY cells were generated using oligo microarrays. Profiles were compared to SH-EP and KELLY cells transfected with either control miRNA or miR-331-3p mimic, and genes with expression changes of at least 2-fold in both cell lines were identified. There was little overlap between genes regulated in cells expressing either miR-885-5p or miR-331-3p (8 upregulated and 28 downregulated genes, Supplementary Tables S1 and S2). Several p53 target genes, *IGFBP3*, *ZMAT3*, *TNFRSF10B*, *BTG3*, *PPAP2B*, *PPM1D*, *RRM2B*, *PTPRE* and *DLC1*, were upregulated in miR-885-5p transfectants²³ (Table 1). Only one p53 target, *GDF15*, was upregulated in miR-331-3p transfectants. *IGFBP3* and *ZMAT3* were among the top-5 genes upregulated in KELLY cells after miR-885-5p expression. These data implicate p53-directed transcriptional changes in the downstream effects of miR-885-5p in neuroblastoma cells. We used the expression profiles of miR-885-5p transfectants to assess expression of genes controlling p53 transcription either positively or negatively. Several genes known to positively regulate p53, namely *DYRK2*, *HIPK2*, and *GAS1*, were upregulated after miR-885-5p expression. Enforced miR-331-3p expression altered expression of none of these genes, but did suppress the positive p53 regulator, *PML* (Supplementary Table S2).

To validate that miR-885-5p upregulated p53 target genes are dependent on functional p53 we additionally profiled Kelly cells 3 days after miR-885-5p or miR-331 transfections in the presence of p53 targeting siRNA or control siRNA. We observed that from nine p53 target genes that emerged

from the first profiling series (Table 1), seven validated miR-885-5p-induced genes (*IGFBP3*, *BTG3*, *ZMAT3*, *PPAP2B*, *PPM1D*, *RRMB2*, *PTPRE*) showed a lack or reduced induction in the presence of p53 targeting siRNA in Kelly cells (Supplementary Table S3), indicating that miR-885-5p induces these genes via increasing p53 transcriptional activity in these cells.

We further tested whether genes downregulated after enforced miR-885-5p expression were enriched for potential miR-885-5p targets compared with upregulated genes, based on the presence of at least one miR-885-5p potential binding site in the 3'UTR detected by *in silico* prediction. We found 74 downregulated genes (10.7%) as compared to only 3 upregulated genes (0.9%, Supplementary Table S1). *CDK2* was among the downregulated genes, identified as a miR-885-5p target here (Figure 3b; Supplementary Figure S4), as was caspase-3 (*CASP3*), β -catenin (*CTNNB1*), citron rho-interacting kinase (*CIT*), farnesyl transferase (*FNTA*) and microphthalmia-associated transcription factor (*MITF*). Genes downregulated after miR-331-3p expression similarly included putative miR-331-3p targets harboring miR-331-3p binding sites (90 genes, 15.6%, Supplementary Table S3). These included *PML*, the serine/threonine-protein kinase, *PIM1*, neurobeachin (*NBEA*), the nerve growth factor receptor, *NGFR* and *ERBB2*, which has also recently been reported to be a miR-331-3p target²⁴. Nineteen (8.2%) of the genes upregulated after miR-331-3p expression also contain miR-331-3p target sites (Supplementary Table S2). This distribution of prospective target genes within the genes regulated after enforced miR-331-3p expression makes less sense that those among the genes regulated after enforced miR-885-5p expression. Together with the lack of apparent phenotype in miR-331-3p-transfected neuroblastoma cells, these results support a less specific role for miR-331-3p in directing changes in the neuroblastoma cell phenotype.

Taken together, these data indicate that miR-885-5p expression activates p53 pathway in neuroblastoma cells, including the induction of p53 and p53 downstream pathway activity, but multiple pathways can be employed by miR-885-5p during regulation of neuroblastoma cell phenotype especially in *TP53* mutant background.

Discussion

In this report, we provide evidence that *miR-885-5p* is a candidate neuroblastoma tumor suppressor and involved in directing the neuroblastoma cell phenotype. Several genomic regions have been characterized that are commonly lost in neuroblastoma, although, the genes responsible for tumor suppression still remain unidentified. Region 3p25.3 is deleted in approximately 14% of neuroblastomas, and is the location of *miR-885-5p*. We show that *miR-885-5p* functions as an inhibitor of proliferation and survival, and positively regulates the p53 pathway. We present data for CDK2 and MCM5 being direct targets of *miR-885-5p*.

Initially, two miRNAs, *miR-885-5p* and *miR-331-3p*, were chosen as candidate tumor suppressive miRNAs in neuroblastoma. Our findings show that *miR-885-5p* is downregulated in neuroblastoma tumors with heterozygous deletion of 3p25.3, and that expression in neuroblastoma cell lines is low or absent also independent of 3p loss. Expression of *miR-331-3p* correlates inversely with amplified *MYCN* in neuroblastoma tumors, but no such trend was detected in neuroblastoma cell lines. Only experimentally enforced expression of *miR-885-5p*, but not *miR-331-3p*, in neuroblastoma cell lines resulted in growth inhibition, senescence and apoptosis. Clearly, *miR-885-5p* fulfills the criteria of a tumor suppressor gene in the context of neuroblastoma.

A master gene orchestrating cell cycle arrest, programmed cell death and senescence is *TP53*. We provide evidence for p53 involvement in *miR-885-5p*-driven cell cycle arrest, senescence and apoptosis. Neuroblastoma cells having wild-type *TP53* displayed G₁-arrest coupled with p53 and p21^{waf1} induction upon *miR-885-5p* introduction. What genes are targeted by *miR-885-5p* to create this phenotype? Among six candidates, CDK2 and MCM5 met the *miR-885-5p* target criteria: (1) they were downregulated upon *miR-885-5p* introduction in all cell lines examined (2) predicted *miR-885-5p* binding sites in their 3'UTRs reduced expression of a reporter construct in the presence of *miR-885-5p*.

It has been described that CDK2 and MCM5 are linked to negative regulation of p53 pathway activity^{21,22}. In our study we found prominent phenotypic similarity between enforced miR-885-5p expression and siRNA-mediated CDK2/MCM5 knockdown in *TP53* wild-type neuroblastoma cells (SH-EP, IMR32 and KELLY). Consistently, antimiR targeting endogenous miR-885-5p elevated the levels of CDK2 and MCM5 and reduced p53 and its downstream targets. In addition, siRNA-mediated p53 knockdown reverted phenotypic as well as protein and transcriptome changes induced by miR-885-5p. Together, this indicates that CDK2 and MCM5 inhibition executes miR-885-5p-mediated growth inhibition in *TP53* wild-type neuroblastoma cells at least in part via p53 induction. Importantly, miR-885-5p did not affect deregulated MYCN expression in *MYCN* amplified neuroblastoma cells. Deregulated MYC proteins modulate p53 function by transcriptionally inhibiting p21^{waf1} leading to an impaired G₁/G₀ arrest²⁵. Our data now indicate that miR-885-5p restores p21^{waf1} function leading to G₁/G₀ arrest in *TP53* wild-type neuroblastoma cells despite high MYCN levels. This miR-885-5p-mediated effect is mainly achieved through targeting of CDK2, because primarily CDK2 and not MCM5 knockdown exerts G₁/G₀ arrest and p21^{waf1} induction similar to those induced by miR-885-5p. An interesting question is why miR-885-5p also triggers apoptosis and senescence in neuroblastoma cells with mutant *TP53*. Such cells cannot engage p53 in response to CDK2 inhibition, which is the cause of G₀/G₁-arrest failure in these cells. However, CDK2 may still act as prosurvival signal in a *TP53* mutant background, as demonstrated by CDK2 knockdown in HDN33 cells. Alternatively, the other arm of miR-885-5p action, MCM5 inhibition, may prevail in *TP53* mutant cells inducing a senescence-like process and G₂/M phase arrest, as evidenced by MCM5 knockdown in HDN33 cells. However, other miR-885-5p targets may influence growth and survival in p53-mutant neuroblastoma. A model of how miR-885-5p function in neuroblastoma cells in the context of targeting CDK2 and MCM5 is proposed in Figure 7.

In addition, our data provide indirect evidence that caspase-3 might be targeted by miR-885-5p. In the presence of elevated p53 protein levels, we found only moderate upregulation of caspase-3 activity,

reduction of procaspase-3 protein with no significant presence of its mature form as well as downregulation of *CASP3* upon miR-885-5p introduction in neuroblastoma cells. According to miRanda algorithm *CASP3* 3'UTR contains a miR-885-5p binding site. Intriguingly, caspase-3 can be involved in degradation of p21^{waf1} ²⁶. We propose that caspase-3 targeting may further determine the response of miR-885-5p-transfected cells, favoring p21^{waf1} accumulation in neuroblastoma cells (Supplementary Figure S5).

Given that, one can speculate about miR-885-5p functions in normal cells; it may withdraw normal cells from cycling via p53 activation but maintain survival. Therefore it would be interesting to determine whether miR-885-5p plays a role in developmental processes, for example, neuronal maturation.

To sum up, our findings lead us to conclude that miR-885-5p engages p53-dependent and independent regulatory layers jointly to interfere with cell cycle progression and survival of neuroblastoma cells. It negatively regulates CDK2 and MCM5 and activates the p53 pathway in *TP53* wild-type neuroblastoma and is able to trigger cell death and senescence in *TP53*-mutant neuroblastoma.

Acknowledgements

The authors thank Gabriele Becker and Yvonne Kahlert for excellent technical assistance, Filip Pattyn for critical remarks and Kathy Astrahantseff for manuscript proofreading. This work was supported with grants N2KR-S19T03 and 01GS0895 within NGFN-2 and NGFN^{Plus} from the BMBF, and the EET-pipeline (#037260) from the EU.

Materials and methods

Patients

Neuroblastoma tumor samples were collected prior to any cytoreductive treatment, snap-frozen and stored at -80°C until RNA or DNA isolation. Written informed consent was obtained from patients' parents for tissue sampling. Genomic *MYCN* status was assessed in the reference laboratories of the German Neuroblastoma trial in Cologne and Heidelberg.

aCGH of primary neuroblastomas and M-FISH

Patient DNA tumor samples (n=193) were analyzed using either 44k (n=143) or 105k (n=51) aCGH microarrays (Agilent Technologies). 2.5 µg each of genomic tumour and reference DNA were used for each hybridization. Labelling and hybridization was performed as previously described²⁷. Arrays were preprocessed using the R/Bioconductor statistical software package. Arrays were segmented using the *daglad* function after lowess normalization, implementing a modified version of the methodology described in Hupe et al.²⁸. Different array platforms were matched using the chromosomal positions of the probes, and missing values were imputed only if two neighbouring probes had the same segmented values. Multicolor FISH (M-FISH) analysis on neuroblastoma cell lines was performed using the 24 XCyte probe-kit (Meta-Systems, Altussheim, Germany). Hybridization was performed according to the manufacturer's instructions. Slides were counterstained with 4,6-diamidino-2-phenylindol (DAPI) (Sigma). Images were captured with a Zeiss Axio Imager Z1 microscope and analysed with Isis/mFISH imaging software (MetaSystems).

Cell culture and transfection

SH-EP, KELLY, IMR32, SK-N-BE(2)c and HDN33 were grown in RPMI supplemented with 10% (v/v) fetal calf serum, 2 mM L-glutamine and 1% (v/v) penicillin/streptomycin in a humidified incubator at 37°C and 5% CO₂. miRNA mimics and anti-miRs were purchased from Ambion. siRNAs to p53, CDK2 and MCM5 and control non-targeting siRNA were purchased from Qiagen, Invitrogen and

Santa Cruz. Cells were plated 24 hours before transient transfection with 30 nM of miRNA mimic or antimiR or Cy3-labeled control miRNA or antimiR using Lipofectamine 2000. siRNA transfections were performed using Lipofectamine 2000 according to manufacturer's instructions. Unless otherwise stated, cells were assayed 4 days after transfection. For p53 knockdown experiments, cells were retransfected with miRNA mimics 24 hours after transfection with p53 siRNA or control siRNA. siRNA transfections were performed using Lipofectamine 2000 according to manufacturer's instructions. To construct the miR-885-5p and miR-331-3p expressing vectors the 500 bp fragments surrounding corresponding miRNA genes were amplified and cloned into the Nhe1 and EcoR1 sites in pcDNA3.1 (Invitrogen). SH-EP and KELLY cells were plated in 6-well plates for stable transfection with 400 µg pcDNA3.1-miR-331-3p, pcDNA3.1-miR-885-5p or empty pcDNA3.1 vector using Effectene (Qiagen). Individual clones were selected that grow in the presence of G418. Stable transfectants were maintained in culture no longer than 4 weeks during experiments.

Clonogenic assay, cell cycle, senescence and apoptosis assays

For cell proliferation evaluation, Alamar Blue (ABD Serotec) was used according manufacturer's instructions. Fluorescence was detected using the FluorStar Optima microplate fluorescence reader (BMG Labtech). The cell cycle distribution was determined as previously described²⁹. To assay for senescence, cells were fixed and stained using the SA-β-Gal kit (Cell Signaling Technology) according to the manufacturer's instructions. Three fields containing 100 cells were counted for each experiment and the results of three independent experiments are presented. Apoptosis was evaluated in FACS analysis by the extent of DNA fragmentation and by extent of phosphatidylserine externalization using FITC Annexin V Detection kit (BD Pharmingen)^{30, 31}.

Soft agar assay

Cells were trypsinised 18 hours after miRNA mimic transfection, and 10^5 cells were resuspended in a top agar solution containing 0.35% noble agar, then poured onto a base layer containing 0.5% agar in

6-well plates. Each well was covered with 3 ml of RPMI full medium, and incubated under standard culture conditions for two weeks. Colonies were fixed and stained with 10% methanol, 10% acetic acid, and 0.5% crystal violet. The colony counting was performed using ImageJ software.

Luciferase reporter assay

miRNA-3'UTR binding sites were predicted by miRanda (www.microrna.org) and Targetscan (www.targetscan.org) algorithms. 3'UTR database was obtained from UTRResource (<http://www.ba.itb.cnr.it/UTR/>)³². pmiRGLO vector (Promega) was used for reporter assay according to manufacturer' instructions. Putative miR-885-5p target sites in the CDK2 and MCM5 3'UTRs were cloned into pmiRGLO vector downstream of the firefly luciferase gene in pmiRGLO vector to create reporter plasmids. The sequences containing miR-885-5p predicted binding sites were used to construct pmiRGLO-CDK2-site are listed in the Supplementary Table S4.

Cells were plated in 96-well plates, and transfected with 20 ng of either pmiRGLO empty, pmiRGLO-CDK2-site, pmiRGLO-CDK2-mut-site, pmiRGLO-MCM5-site or pmiRGLO-MCM5-mut-site using Effectene (Qiagen), or miRNA mimics. Cells were lysed in passive cell lysis buffer (Promega) 24 hours post-transfection, and lysates were processed using the Dual-Luciferase Reporter Assay System (Promega) according to the manufacturer's directions. Luciferase activity was detected in a FluorStar Optima microplate fluorescence reader. Firefly luciferase activity was normalized to Renilla luciferase activity as an internal transfection control. Transfections were performed in six independent experiments, and assayed in duplicate.

RT-qPCR

TaqMan miRNA assays (Applied Biosystems) were used to quantify endogenous miR-885-5p and miR-331-3p. RNA was isolated from neuroblastoma cell lines using TRIzol, and 5 ng of total RNA was used to reverse transcribe cDNA for miRNA assessment. Data from cell lines were normalized to U44 RNA expression. miRNA expression in primary tumor samples was analysed as previously described³³, and normalization was performed by using a set of miRNAs stably expressed in neuroblastomas. Real-

time RT-PCR was performed by using the Applied Biosystems 7000 Sequence Detection system (Applied Biosystems).

Northern Blotting

Northern Blotting was performed as previously described¹². Total RNA was isolated with TRIZOL reagent (Invitrogen). 30 µg of total RNA was loaded per lane and separated on 15% denaturing polyacrylamide gels, transferred by electroblotting to GeneScreen+ membranes (Perkin Elmer). Methylene blue staining was performed prior to blocking with ULTRAhyb-Oligo hybridization buffer (Ambion) to assess RNA loading. Blots were incubated with 10 ng/ml 3'-biotinylated DNA probes complementary to either miR-885-5p or miR-331-3p in ULTRAhyb-Oligo buffer then visualized using the North2South Chemiluminescent Hybridization and Detection Kit (Pierce).

Western Blotting

Whole cells were lysed in a buffer containing 7 M urea, 1% Triton X-100, 100 mM DTT, 20 mM Tris-HCl, pH 8.5. Protein concentrations were determined by Bradford assay (Bio-Rad), and 20 µg protein lysate were separated per lane on either 12% or 15% PAGE gels then transferred to nitrocellulose membranes (Protran). Antibody to MCM5 was purchased from Abcam. Antibody to PUMA was from ProSci Inc. Antibodies to p53, MCM3, STAT3, E2F1, MYCN, CUL3 and β-actin were from Santa Cruz Biotechnologies. Antibodies to p27, CDK2, CDK6 were from Dianova. Antibodies to precursor and mature CASP3 were from BD Transduction Laboratories and Cell Signaling, respectively. HRP-conjugated antibodies against mouse or rabbit were obtained from Jackson Immunoresearch. Sheep anti-goat HRP-conjugated antibody was from Santa Cruz Biotechnologies. Membranes were incubated with the appropriate antibodies, and bands were visualized using the ECL system (Pierce). Images were captured with a CCD camera (Vilber Lourmat) and densitometry analysis was performed using ImageJ software.

Gene expression analysis

In the first series of experiments, RNA was isolated from cells 3 days after transient transfection with

miR-885-5p, miR-331-3p, or control miRNA. In a second series of experiments, RNA was isolated from cells pretreated with p53 siRNA or control siRNA for 1 day and subsequently transfected with miR-885-5p, miR-331-3p, or control miRNA for 3 days. Gene expression profiles were generated as two one-color replicates using the whole genome oligonucleotide microarray platform from Agilent (Agilent Technologies) as previously described^{34, 35}. Raw microarray data were normalized using quantile normalization. Expression ratios are given as the mean of two replicates. All raw and normalized microarray data are available at the ArrayExpress database (<http://www.ebi.ac.uk/arrayexpress>; Accession: E-TABM-38) or iCHIP (www.ichip.de/).

Statistical analysis

Statistical significance was calculated using the Student t-test. Data are presented as mean±SD from at least three experiments.

References

1. Lu J, Getz G, Miska EA, Alvarez-Saavedra E, Lamb J, Peck D, Sweet-Cordero A, Ebert BL, Mak RH, Ferrando AA, Downing JR, Jacks T, Horvitz TR, Golub TR. MicroRNA expression profiles classify human cancers. *Nature* 2005; 435: 834–838.
2. Calin GA, Sevignani C, Dumitru CD, Hyslop T, Noch E, Yendamuri S, Shimizu M, Rattan S, Bullrich F, Negrini M, Croce CM. Human microRNA genes are frequently located at fragile sites and genomic regions involved in cancers. *Proc Natl Acad Sci USA* 2004; 101: 2999-3004.
3. Calin GA, Dumitru CD, Shimizu M, Bichi R, Zupo S, Noch E, Aldler H, Rattan S, Keating M, Rai K, Rassenti L, Kipps T, Negrini M, Bullrich F, Croce CM. Frequent deletions and down-regulation of microRNA genes mir-15 and mir-16 at 13q14 in chronic lymphocytic leukemia. *Proc Natl Acad Sci USA* 2005; 99: 15524-15529.
4. Chang T-C, Wentzel EA, Kent OA, Ramachandran K, Mullendore M, Lee KH, Feldmann G, Yamakuchi M, Ferlito M, Lowenstein CJ, Arking DE, Beer MA, Maitra A, Mendell JT. Transactivation of mir-34a by p53 Broadly Influences Gene Expression and Promotes Apoptosis. *Mol Cell* 2007; 26: 745–752.
5. Welch C, Chen Y, Stallings RL. MicroRNA-34a functions as a potential tumor suppressor by inducing apoptosis in neuroblastoma cells. *Oncogene* 2007; 26: 5017–5022.
6. Westermann F, Schwab M. Genetic parameters of neuroblastomas. *Cancer Lett* 2002; 184: 127-147.
7. Schwab M, Westermann F, Hero B, Berthold F. Neuroblastoma: biology and molecular and chromosomal pathology. *Lancet Oncol* 2003; 4: 472-480.
8. McKenzie PP, Guichard SM, Middlemas DS, Ashmun RA, Danks MK, Harris LC. Wild-type p53 can induce p21 and apoptosis in neuroblastoma cells but the DNA damage-induced G1 checkpoint function is attenuated. *Clin Cancer Res* 1999; 5: 4199-4207.
9. Van Maerken, Vandesompele, J., Rihani, A., De Paepe, A., Speleman, F. Escape from p53-

mediated tumor surveillance in neuroblastoma: switching off the p14^{ARF}-MDM2-p53 axis. *Cell Death Diff* 2009; 16: 1563-1572.

10. Plantaz D, Vandesompele J, Van Roy N, Łastowska M, Bown N, Combaret V, Favrot MC, Delattre O, Michon J, Benard J, Hartmann O, Nicholson JC, Ross FM, Brinkschmidt C, Laureys G, Caron H, Matthay KK, Feuerstein BG, Speleman F. Comparative genomic hybridization (CGH) analysis of stage 4 neuroblastoma reveals high frequency of 11q deletion in tumors lacking MYCN amplification. *Int J Cancer* 2001; 91: 680 – 686.

11. Hoebeek J, Vandesompele J, Nilsson H, De Preter K, Van Roy N, De Smet E, Yigit N, De Paepe A, Laureys G, Pålman S, Speleman F. The von Hippel-Lindau tumor suppressor gene expression level has prognostic value in neuroblastoma. *Int J Cancer* 2006; 119: 624–629.

12. Afanasyeva EA, Hotz-Wagenblatt A, Glatting KH, Westermann F. New miRNAs cloned from neuroblastoma. *BMC Genomics* 2008; 9: 52.

13. Tweddle DA, Malcolm AJ, Bown N, Pearson AD, Lunec J. Evidence for the development of p53 mutations after cytotoxic therapy in a neuroblastoma cell line. *Cancer Res* 2001; 61: 8-13.

14. Fukasawa K, Choi T, Kuriyama R, Rulong S, Van de Woude GF. Abnormal centrosome amplification in the absence of p53. *Science* 1996; 271: 1744-1747.

15. Carroll PE, Okuda M, Horn FH, Biddinger P, Stambrook PJ, Gleich LL, Li Y-Q, Tarapore P, Fukasawa K. Centrosome hyperamplification in human cancer: chromosome instability induced by p53 mutation and/or Mdm2 overexpression. *Oncogene* 1999; 18: 1935-1944.

16. Betel D, Wilson M, Gabow A, Marks DS, Sander C. The microRNA.org resource: targets and expression. *Nucleic Acids Res* 2008; 36: D149-153.

17. Lewis BP, Burge CB, Bartel DB. Conserved seed pairing, often flanked by adenosines, indicates that thousands of human genes are microRNA targets. *Cell* 2005; 120: 15-20.

18. John B, Enright AJ, Aravin A, Tuschl T, Sander C, Marks DS. Human microRNA targets.

PLOS Biol 2005; 3: e264.

19. Darnowski JW, Goulette FA, Guan JJ, Chatterjee D, Yang Y-F, Cousens LP, Chin YE. STAT3 cleavage by caspases: impact on full-length STAT3 expression, fragment formation and transcriptional activity. *J Biol Chem* 2006; 281: 17707-17717.
20. Schwab BL, Leist M, Knippers R, Nicotera P. Selective proteolysis of the nuclear replication factor MCM3 in apoptosis. *Exp Cell Res* 1998; 238: 415-421.
21. Agarwal MK, Amin ARMR, Agarwal ML. DNA replication licensing factor Minichromosome Maintenance Deficient 5 rescues p53-mediated growth arrest. *Cancer Res* 2007; 67: 116-121.
22. Molenaar JJ, Ebus ME, Geerts D, Koster J, Lamers F, Valentijn LJ, Westerhout E M, Versteeg R, Caron HN. Inactivation of CDK2 is synthetically lethal to MYCN over-expressing cancer cells. *Proc Natl Acad Sci USA* 2009; 106: 12968-12973.
23. Wei CL, Qiang W, Vega VB, Chiu KP, Ng P, Zhang T, Shahab A, Yong HC, Fu Y, Weng Z, Liu J, Zhao XD, Chew JL, Lee YL, Kuznetsov VA, Sung W-K, Miller LD, Lim B, Liu ET, Yu Q, Ng H-H, Ruan Y. A Global Map of p53 Transcription-Factor Binding Sites in the Human Genome. *Cell* 2006; 124: 207-219.
24. Epis MR, Giles KM, Barker A, Kendrick TS, Leedman PJ. mir-331-3p regulates ERBB-2 expression and androgen receptor signaling in prostate cancer. *J Biol Chem* 2009; 284: 24696-24704.
25. Seoane J., Le H.-V., Massague J. Myc suppression of the p21 Cip1 Cdk inhibitor influences the outcome of the p53 response to DNA damage. *Nature* 2002 419: 729-734.
26. Levkau B, Koyama H, Raines EW, Clurman BE, Herren B, Orth K, Roberts JM, Ross R. Cleavage of p21Cip1/Waf1 and p27Kip1 mediates apoptosis in endothelial cells through activation of Cdk2: role of a caspase cascade. *Mol Cell* 1998 1: 553–563.
27. Spitz R, Oberthuer A, Zapatka M, Brors B, Hero B, Ernestus K, Oestreich J, Fischer M, Simon T, Berthold F. Oligonucleotide array-based comparative genomic hybridization (aCGH) of 90 neuroblastomas reveals aberration patterns closely associated with relapse pattern and outcome. *Genes*

Chromosomes Cancer 2006; 45: 1130-1142.

28. Hupé P, Stransky N, Thiery JP, Radvanyi F, Barillot E. Analysis of array CGH data: from signal ratio to gain and loss of DNA regions. *Bioinformatics* 2004; 20: 3413-3422.

29. Deubzer HE, Ehemann V, Westermann F, Heinrich R, Mechttersheimer G, Kulozik AE, Schwab M, Witt O. Histone deacetylase inhibitor Helminthosporium carbonum (HC)-toxin suppresses the malignant phenotype of neuroblastoma cells. *Int J Cancer* 2008; 122: 1891-1900.

30. Nicoletti I, Migliorati G, Pagliacci MC, Grignani F, Riccardi C. A rapid and simple method for measuring thymocyte apoptosis by propidium iodide staining and flow cytometry. *J Immunol Methods* 1991; 139: 271-279.

31. Koopman G, Reutelingsperger CP, Kuijten GA, Keehnen RM, Pals ST, van Oers MH. Annexin V for flow cytometric detection of phosphatidylserine expression on B cells undergoing apoptosis. *Blood*. 1994; 84:1415-1420.

32. Mignone F, Grillo G, Licciulli F, Iacono M, Liuni S, Kersey PJ, Duarte J, Saccone C, Pesole G. UTRdb and UTRsite: a collection of sequences and regulatory motifs of the untranslated regions of eukaryotic mRNAs. *Nucleic Acids Res* 2005; 33: D141-D146.

33. Mestdagh P, Van Vlierberghe P, De Weer A, Muth D, Westermann F, Speleman F, Vandesompele J. A novel and universal method for microRNA RT-qPCR data normalization. *Genome Biol* 2009; 10: R64.

34. Westermann F, Muth D, Benner A, Bauer T, Henrich KO, Oberthuer A, Brors B, Beissbarth T, Vandesompele J, Pattyn F, Hero B, König R, Fischer M, Schwab M. Distinct transcriptional MYCN/c-MYC activities are associated with spontaneous regression or malignant progression in neuroblastomas. *Genome Biol* 2008; 9: R150.

35. Oberthuer A, Berthold F, Warnat P, Hero B, Kahlert Y, Spitz R, Ernestus K, König R, Haas S, Eils R, Schwab M, Brors B, Westermann F, Fischer M. Customized oligonucleotide microarray gene

expression-based classification of neuroblastoma patients outperforms current clinical risk stratification. *J Clin Oncol* 2006; 24: 5070-5078.

Table 1. miR-885-5p activates p53 transcriptional program

HGNC symbol	Chromosome, Band	Description	HGNC symbol	Chromosome, Band	Description
P53 targets upregulated in miR-885-5p transfectants			P53 targets upregulated in miR-331-3p transfectants		
IGFBP3	7p12.3	Insulin-like growth factor-binding protein 3	GDF15	19p13.11	Growth differentiation factor 15
BTG3	21q21.1	Protein BTG3 (Abundant in neuroepithelium area protein)			
ZMAT3	3q26.32	Zinc finger matrin-type protein 3 (p53-activated gene 608 protein)			
PPAP2B	1p32.2	Lipid phosphate phosphohydrolase 3			
PPM1D	17q23.2	Protein phosphatase 1D (p53-induced protein phosphatase 1)			
TNFRSF10B	8p21.3	Tumor necrosis factor receptor superfamily member 10B			
RRM2B	8q22.3	Ribonucleoside-diphosphate reductase subunit M2 B			
DLC1	8p22	Rho GTPase-activating protein 7 (Deleted in liver cancer 1 protein)			
PTPRE	10q26.2	Receptor-type tyrosine-protein phosphatase epsilon			

Figure legends

Figure 1 – 7

Figure 1. The *miR-885-5p* gene at 3p25.3 is expressed at low level in primary neuroblastomas with segmental 3p loss. (a) Patient characteristics are shown for the 193 primary neuroblastomas analyzed on either 44K or 105K oligo microarrays. The percentage of tumors with heterozygous 3p25.3/*miR-885-5p* deletion are indicated in parenthesis. (b) Expression of miR transcripts were verified using RT-qPCR in 60 primary neuroblastomas, and are shown as box plots. MNA – *MYCN*-amplified neuroblastomas. ΔCq values were multiplied by -1 to represent relative expression of *miR-885-5p* and *miR-331-3p*. *miR-885-5p*: median $\Delta Cq \times -1 = 1.83$, range -0.04 to 6.43; *miR-331-3p*: median $\Delta Cq \times -1 = -7.31$, range -8.57 to -4.35). (c) Neuroblastoma cell lines used in the screen. The *MYCN* amplification, *TP53/INK4a/ARF* and 3p status are listed as reported previously^{13,14} or assessed in this study; * – age of the patient – 10 years, stage – 4. (d) Expression of *miR-885-5p* and *miR-331-3p* was assessed in nine established neuroblastoma cell lines using RT-qPCR (bar graphs). *miR-885-5p* $\Delta Cq \times -1$ median -8.1, range -6.3 to -12.4; *miR-331-3p* $\Delta Cq \times -1$ median -4.3, range -3 to -5.2.

Figure 2. *miR-885-5p* inhibits neuroblastoma proliferation and survival. (a) IMR32, HDN33, SH-EP, KELLY and SK-N-BE(2)c cells were transfected with *miR-885-5p*, *miR-331-3p* mimics, control miRNA (each 30 nM), Lipofectamine 2000 (vehicle) or left untreated. Cell viability was measured by Alamar Blue assay. The data are represented as the means \pm SD (a; insert) SA- β -Gal assays were performed 4 days after transfection; the positively stained cells were counted (mean percentages \pm SD of three experiments are presented). (b) IMR32, SH-EP, KELLY and SK-N-BE(2)c were transfected with miRNA mimics and assayed for anchorage-independent growth in soft agar after two weeks in culture. Colonies were fixed and stained with crystal violet and counted using ImageJ software. The graphs (right) show mean percentages of colonies number \pm SD of three experiments (c) cell cycle profiles of controls and cells transfected with miRNA mimics were determined using FACS analysis. (d) The sub-G₁ fraction of neuroblastoma cell lines transfected with miRNA mimics or control miRNA

transfectants were detected 4 days post-transfection using FACS analysis by detection of cells with a hypodiploid DNA content (bar = mean percentage of sub-G₁ ± SD). Phosphatidylserine externalization was analyzed by annexin V/PI staining, the results show the percentage of annexin V positive/PI negative and annexin V/PI double positive cells.

Figure 3. miR-885-5p induces p53 and downregulates CDK2 and MCM5. (a) (b) Protein expression of several cell cycle and apoptosis regulators, including potential miR-885-5p targets, is shown in western blots of neuroblastoma cells lines 4 days after transfection of miR-885-5p, miR-331-3p or controls. MCM3 cleavage products are indicated (*). Densitometry analysis was performed using ImageJ software; the relative densitometry values are shown on top.

Figure 4. miR-885-5p directly targets CDK2 and MCM5. Predicted miR-885-5p target sites in the CDK2 and MCM5 3'UTRs. Lines indicate perfect matches; colons, G:U pairs. Luciferase reporter assays of stably transfected cells and miRNA-mimic-transfected cells (indicated on x-axis) transiently transfected with either empty vector or vector containing wild-type or mutant miR-885-5p binding sites (indicated as bar color). Firefly luciferase values were normalized to renilla activity. The highest normalized luciferase activity of the stable transfected cells or cells transfected with miRNA mimics was set to 1, and values are reported as fold increase (mean relative luciferase activity ± SD). *, P < 0.1; **, P < 0.05; ***, P < 0.01 versus vector with mutant miR-885-5p binding sites.

Figure 5. CDK2 and MCM5 knockdown mimic miR-885-5p-induced phenotype. (a) IMR32, HDN33, SH-EP, KELLY and SK-N-BE(2)c cells were transfected with anti CDK2 (5 nM), anti MCM5 (5 nM), anti CDK2 (2,5 nM) + anti MCM5 (2,5 nM) siRNAs or control siRNA (5 nM) with Lipofectamine 2000. Cell viability was measured 24h, 48h and 72 h after transfection by Alamar Blue assay. The data are represented as the mean ± SD. (b) siRNA transfected cells were assayed for anchorage-independent growth in soft agar after two weeks in culture. Colonies were counted using ImageJ software (mean percentages of colonies number ± SD of three experiments are presented in the graphs, right). (c) SA-β-Gal assays were performed 4 days after transfection; the positively stained cells

were counted (mean percentages \pm SD of three experiments are presented). Cell cycle profiles of controls and cells transfected with siRNAs were determined using FACS analysis. The sub-G₁ fraction of neuroblastoma cell lines transfected with miRNA mimics or control miRNA transfectants were detected 4 days post-transfection by FACS analysis by detection of cells with a hypodiploid DNA content (bar = mean percentage of sub-G₁ \pm SD). Phosphatidylserine externalization was analyzed by annexin V/PI staining, the percentage of annexin V positive and annexin V/PI double positive cells are indicated. **(d)** protein expression of MCM5, CDK2, p21^{waf1}, p53, PUMA and E2F1 from siRNA transfected cells is shown in western blots. The relative densitometry values are shown.

Figure 6. miR-885-5p-induced growth arrest is p53 dependent in TP53 wild-type neuroblastoma cells **(a)** IMR32, SH-EP and KELLY cells were transfected with siRNA to p53 or control siRNA using Lipofectamine 2000 and transfected with miRNA mimics 24 hours later. p53 knockdown efficiency was evaluated at day 4 after transfection (insert below). Cell viability was measured by Alamar Blue assay for 24h, 48h and 72 h after miRNA mimic transfection (upper panel). The data are represented as the means \pm S.D of three experiments. The cell cycle profiles were performed by FACS analysis (middle panel). **(a, insert)** p53 knockdown efficiency is shown in western blots in IMR32, KELLY, SH-EP. **(b)** p53 knockdown and control siRNA transfected IMR32, KELLY, SH-EP cells were transfected with miRNA mimics and assayed for anchorage-independent growth in soft agar after two weeks in culture. Colonies were fixed and stained with crystal violet and counted using ImageJ software. The graphs show mean percentages of colonies number \pm SD of three experiments. **(c)** protein expression of p21^{waf1}, PUMA and p53 is shown in western blots of p53 knockdown and control siRNA transfected IMR32, KELLY, SH-EP cells 3 days after transfection of miRNA mimics. **(d)** IMR32 and SK-N-BE(2)c were transfected with anti-miR-885-5p or control anti-miR (30 nM) and assayed for anchorage-independent growth for two weeks. Colonies were counted using ImageJ software (mean percentages of colonies number \pm SD of three experiments are presented). Protein

expression of p53, p21^{waf1}, PUMA, CDK2 and MCM5 in anti-miR-transfected IMR32 and SK-N-BE(2)c cells is shown in western blots. The relative densitometry values are shown on top of the western blot panels.

Figure 7. A model for miR-885-5p function.

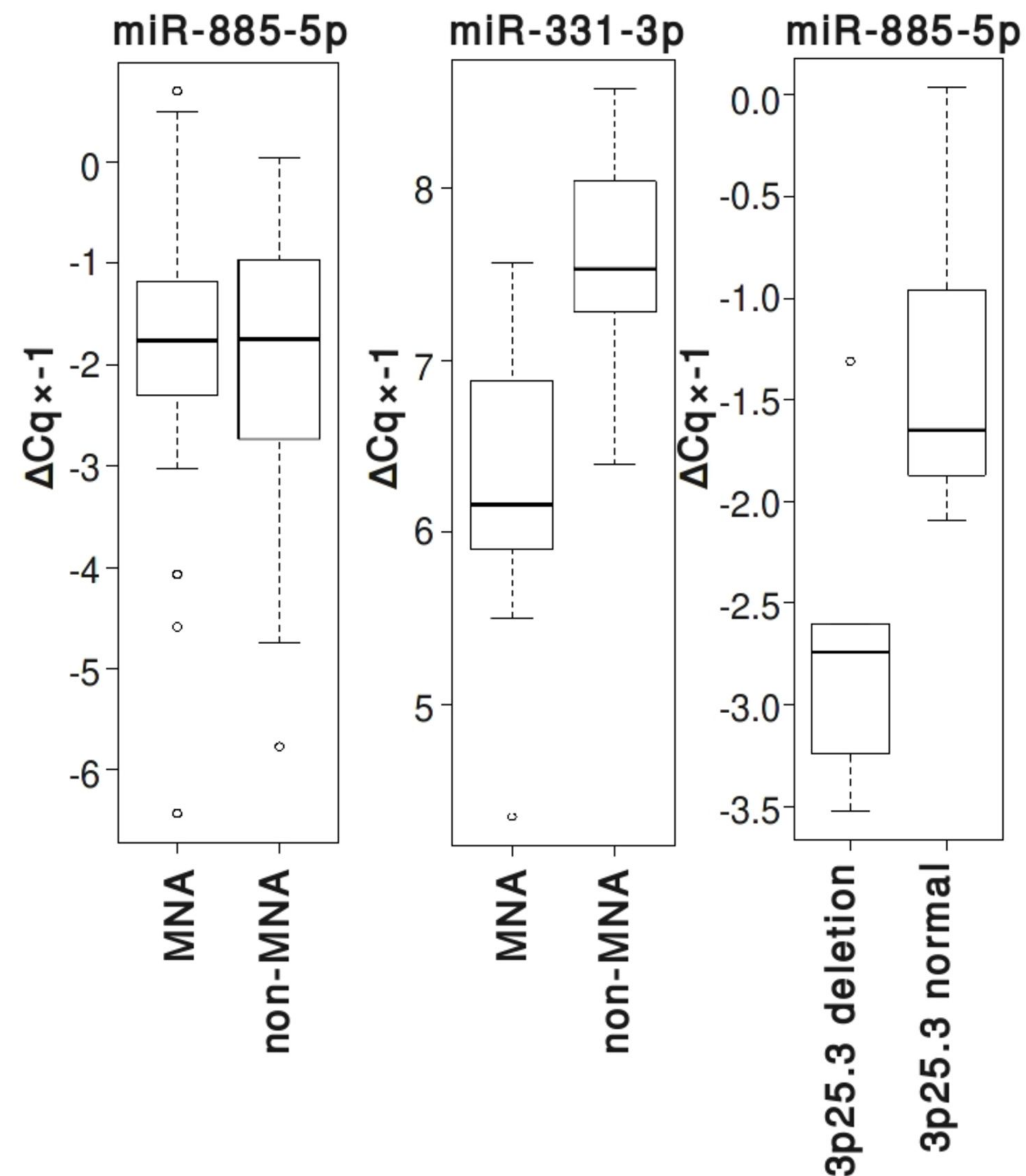
Proposed model for miR-885-5p function via CDK2 and MCM5 downregulation in neuroblastoma. miR-885-5p downregulates CDK2 leading to p53 activation in neuroblastoma cells with wild-type *TP53*. miR-885-5p-triggered CDK2 and MCM5 downregulation reduces cell renewal capacity and favors apoptosis and senescence in neuroblastoma with either wild-type or non-functional *TP53*.

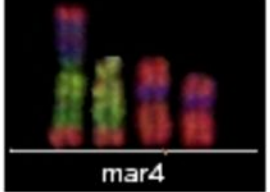
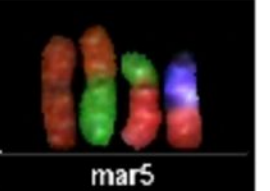

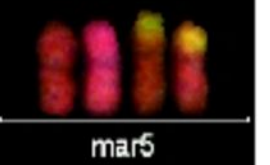
a

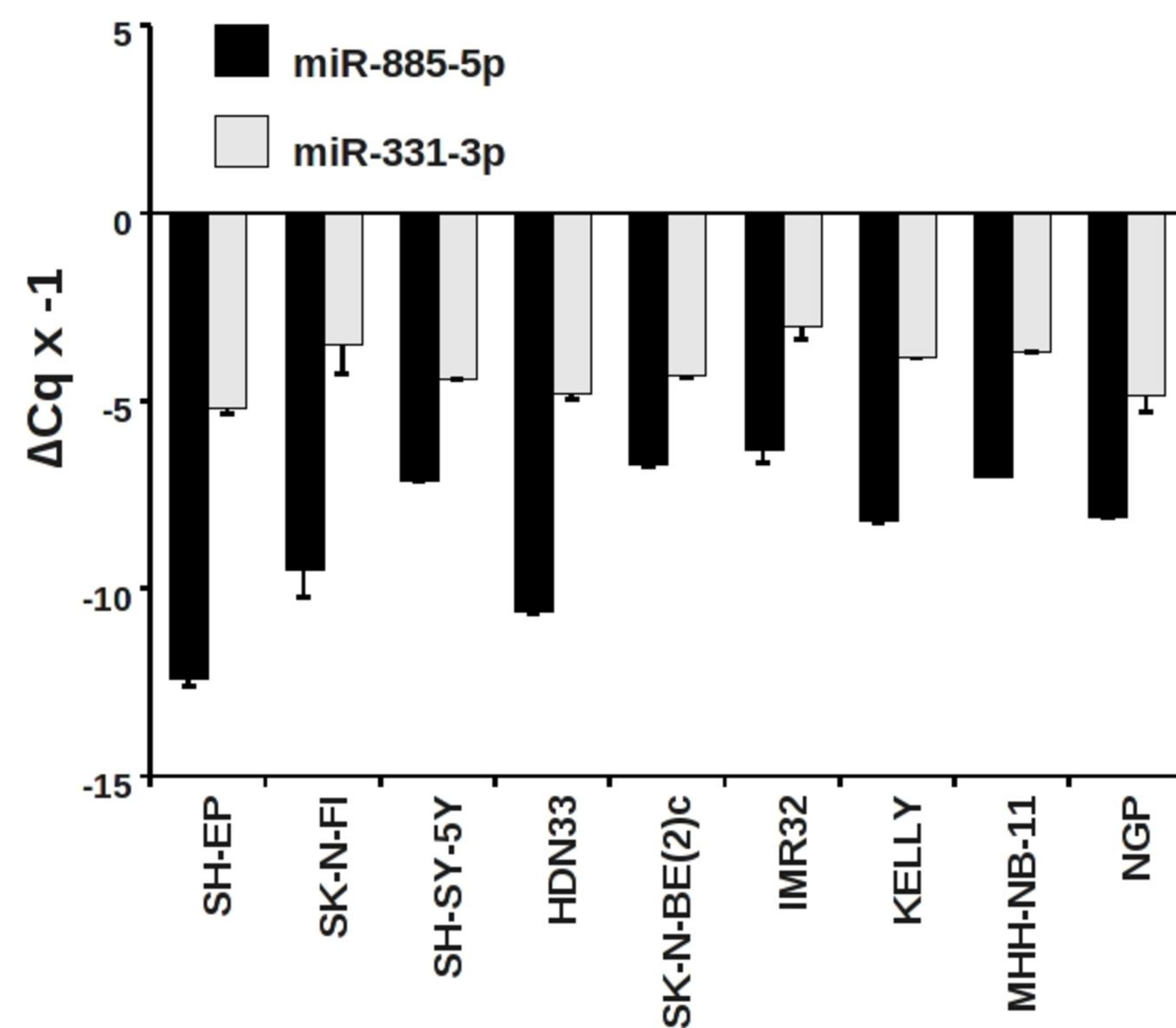
Patient characteristics of CGH cohort

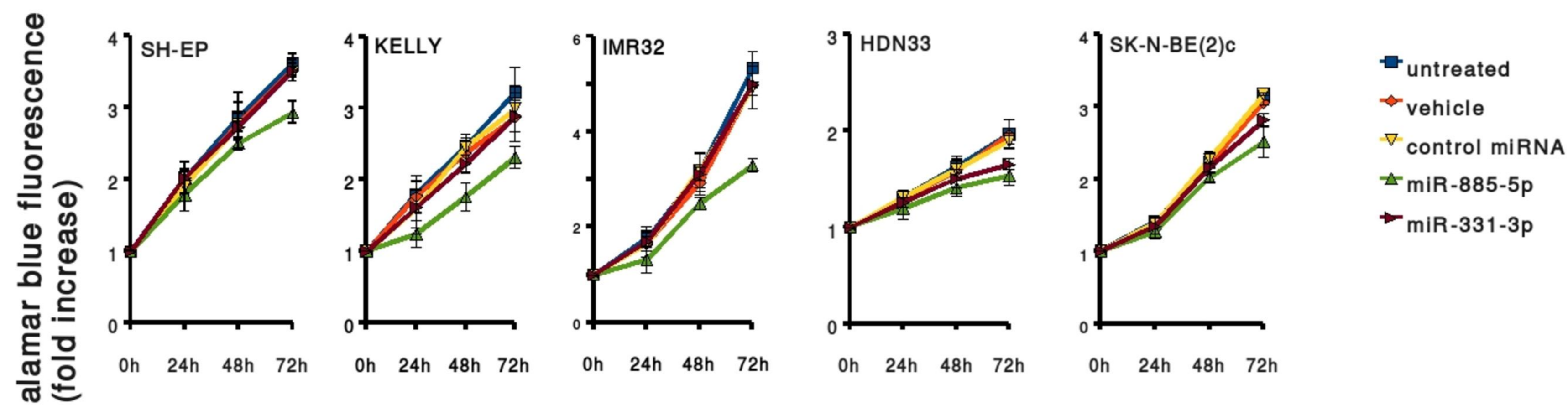
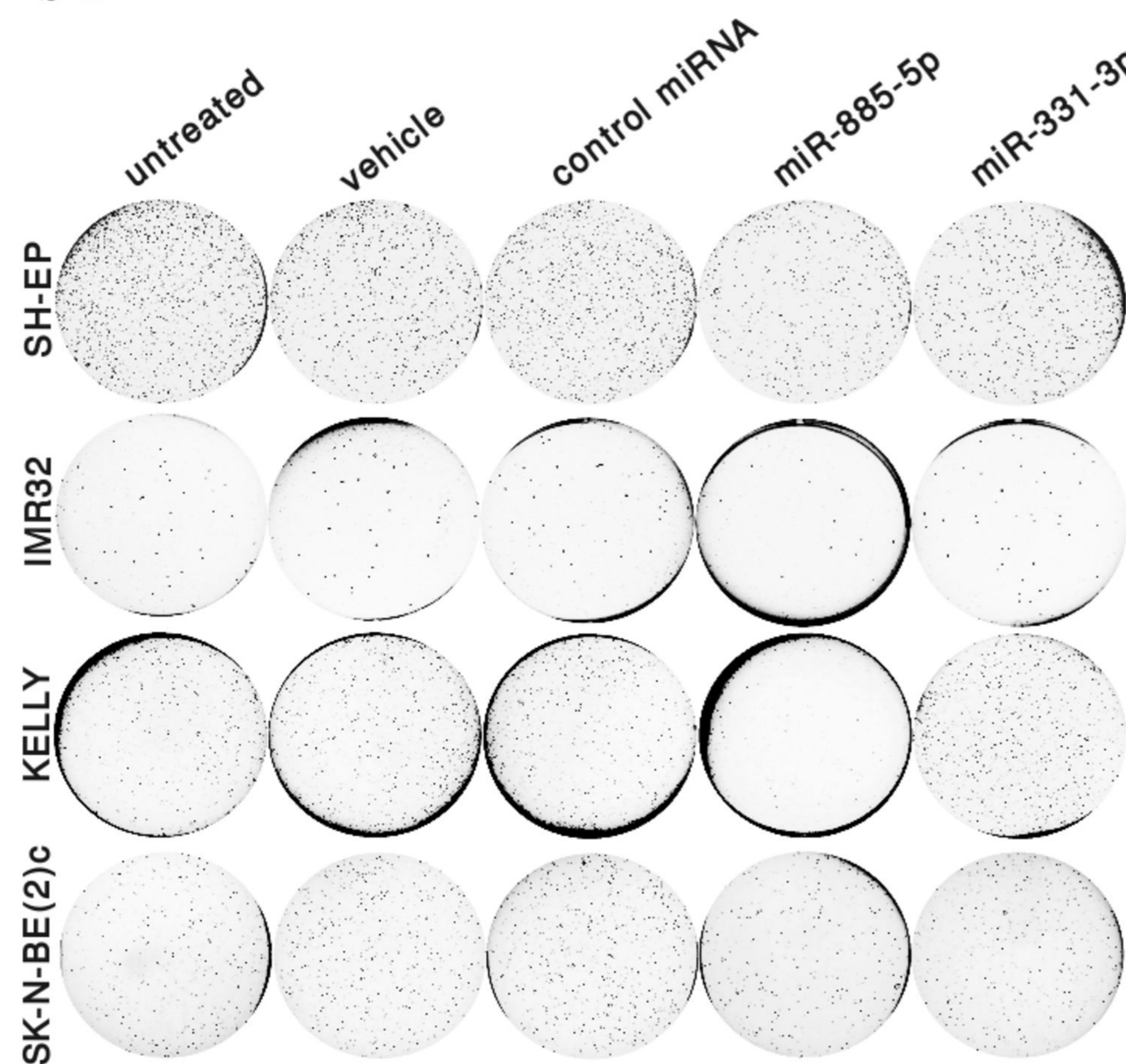
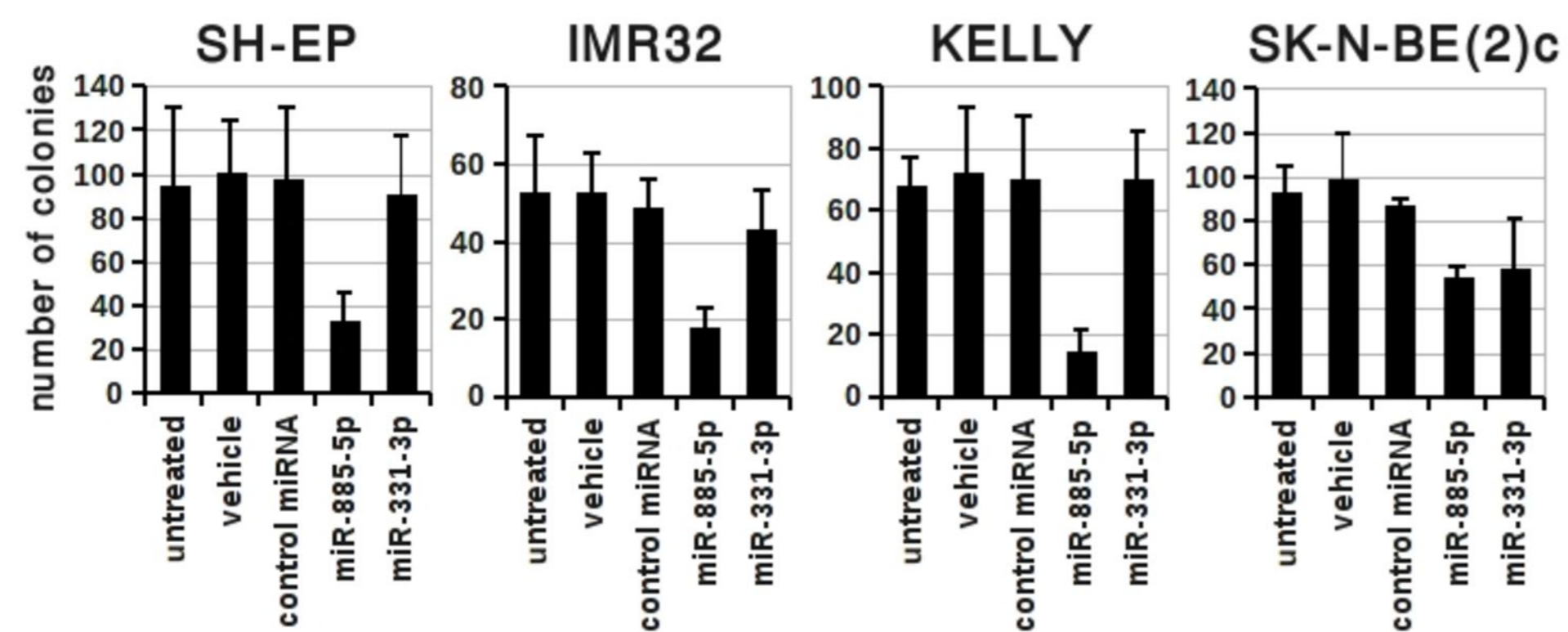
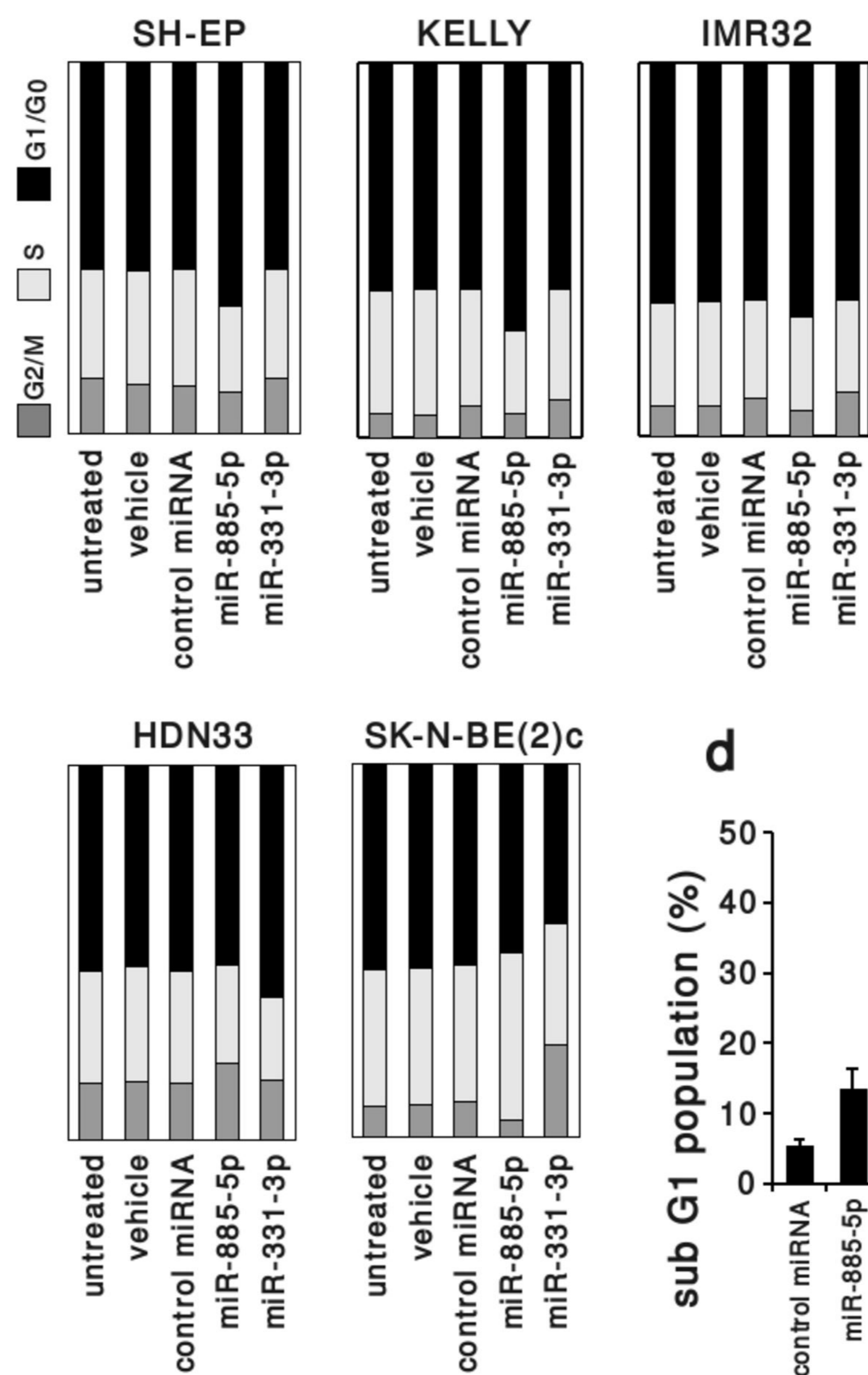
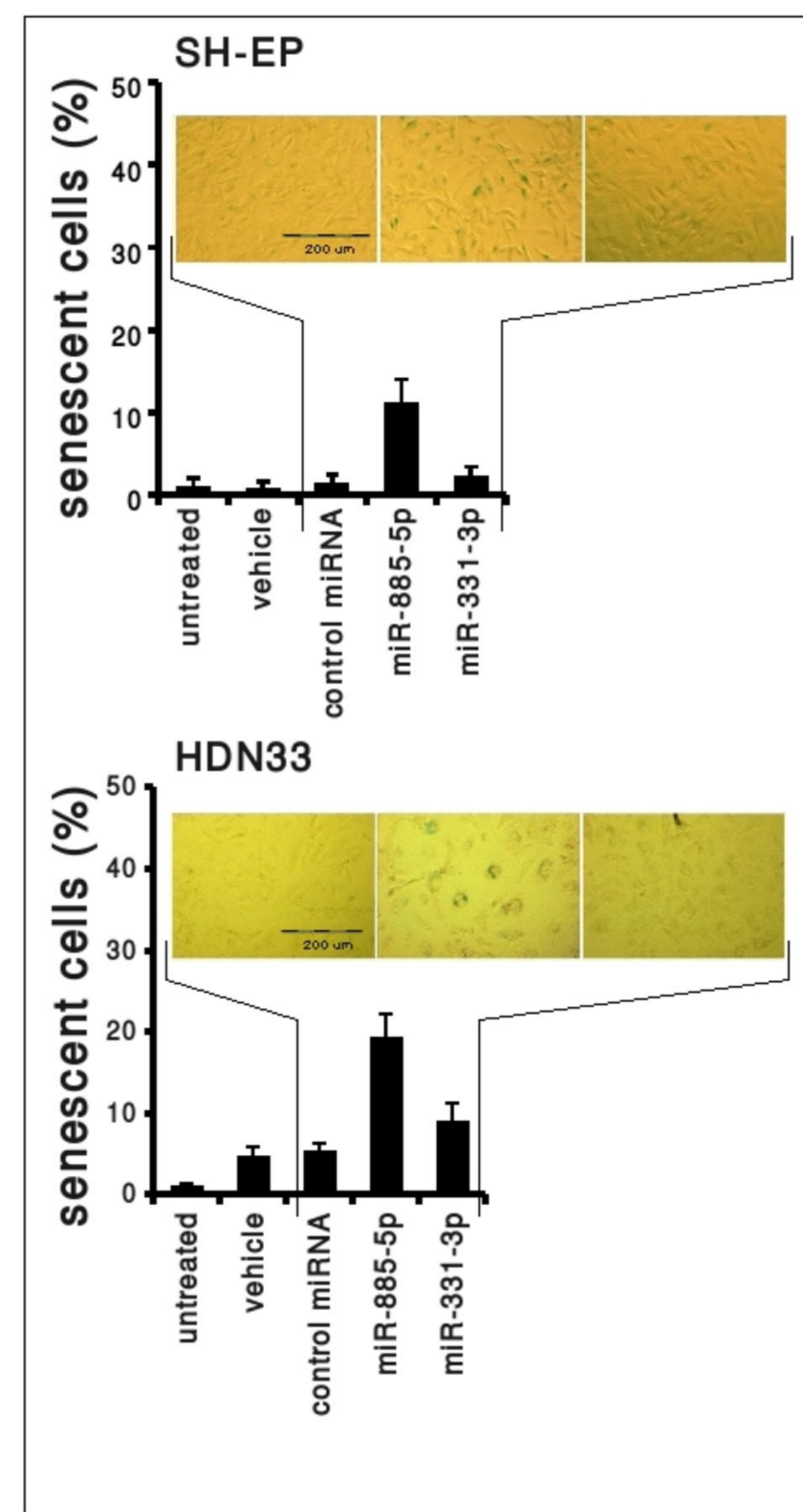
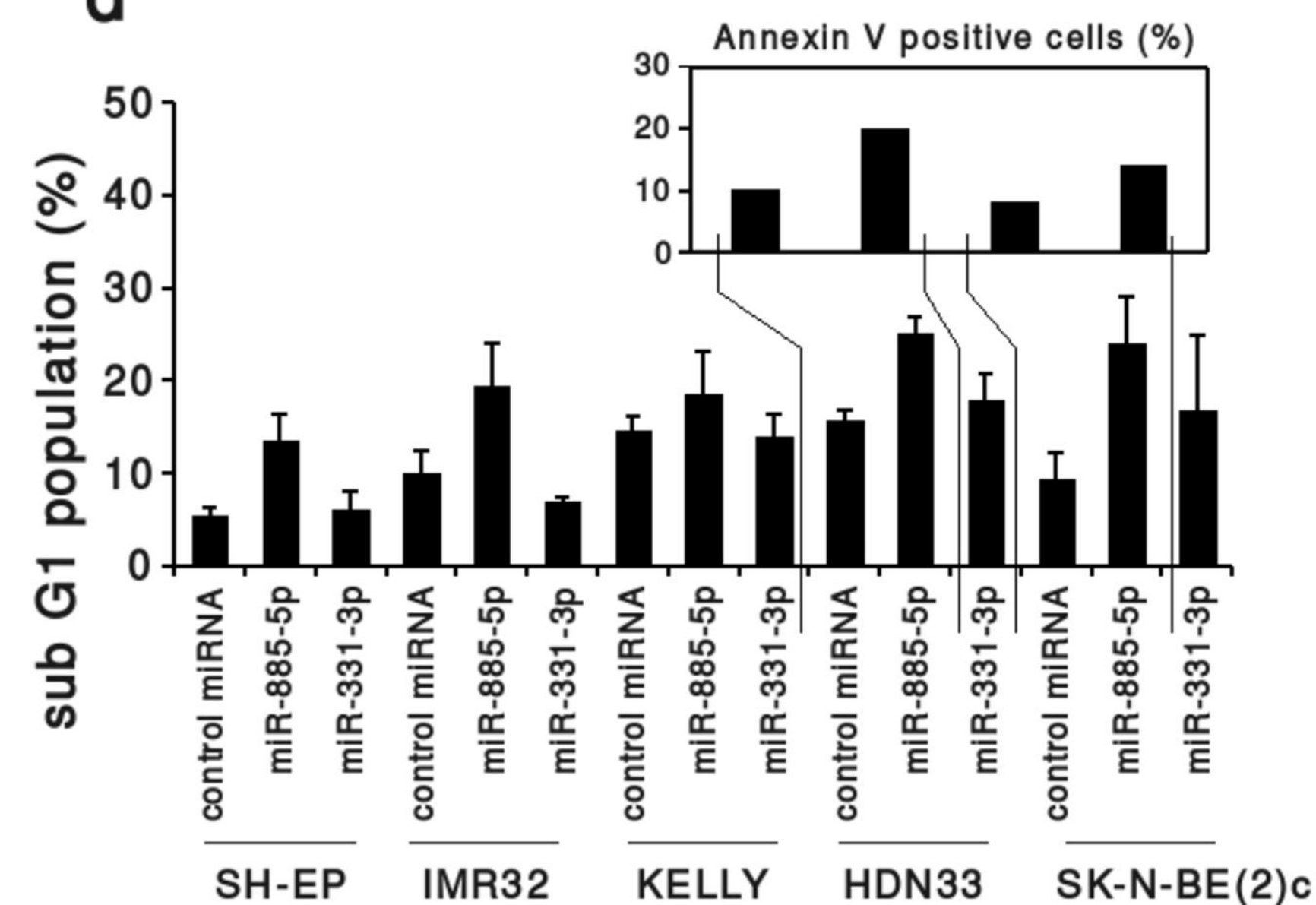
	n (%)
INSS#	
1	33 (17)
2	38 (20)
3	39 (20)
4	61 (32)
4s	22 (11)
MYCN amplification	
No	158 (82)
Yes	35 (18)
3p25.3/miR-885 deletion	
No	166 (86)
Yes	27 (14)
Age (month)	
<18	110
	83
Total	193

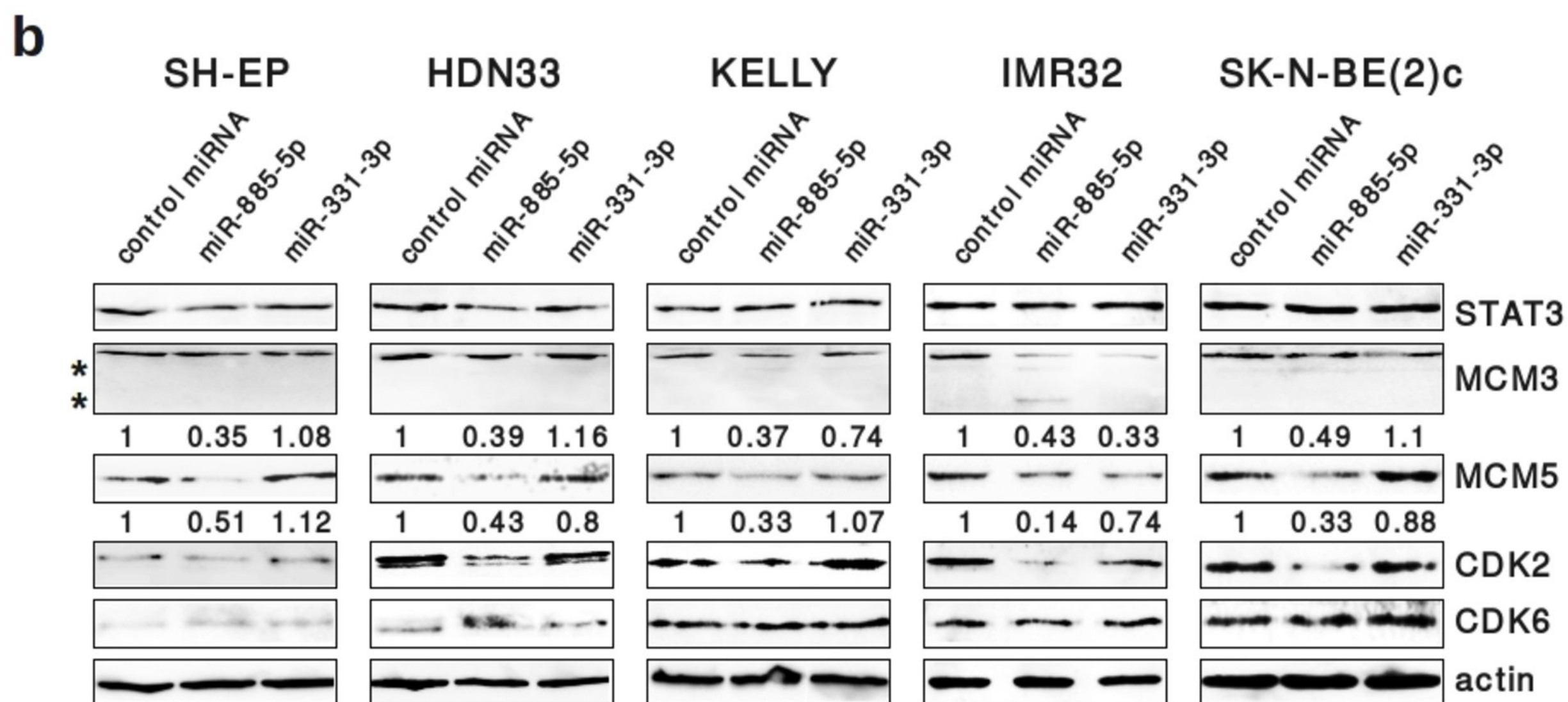
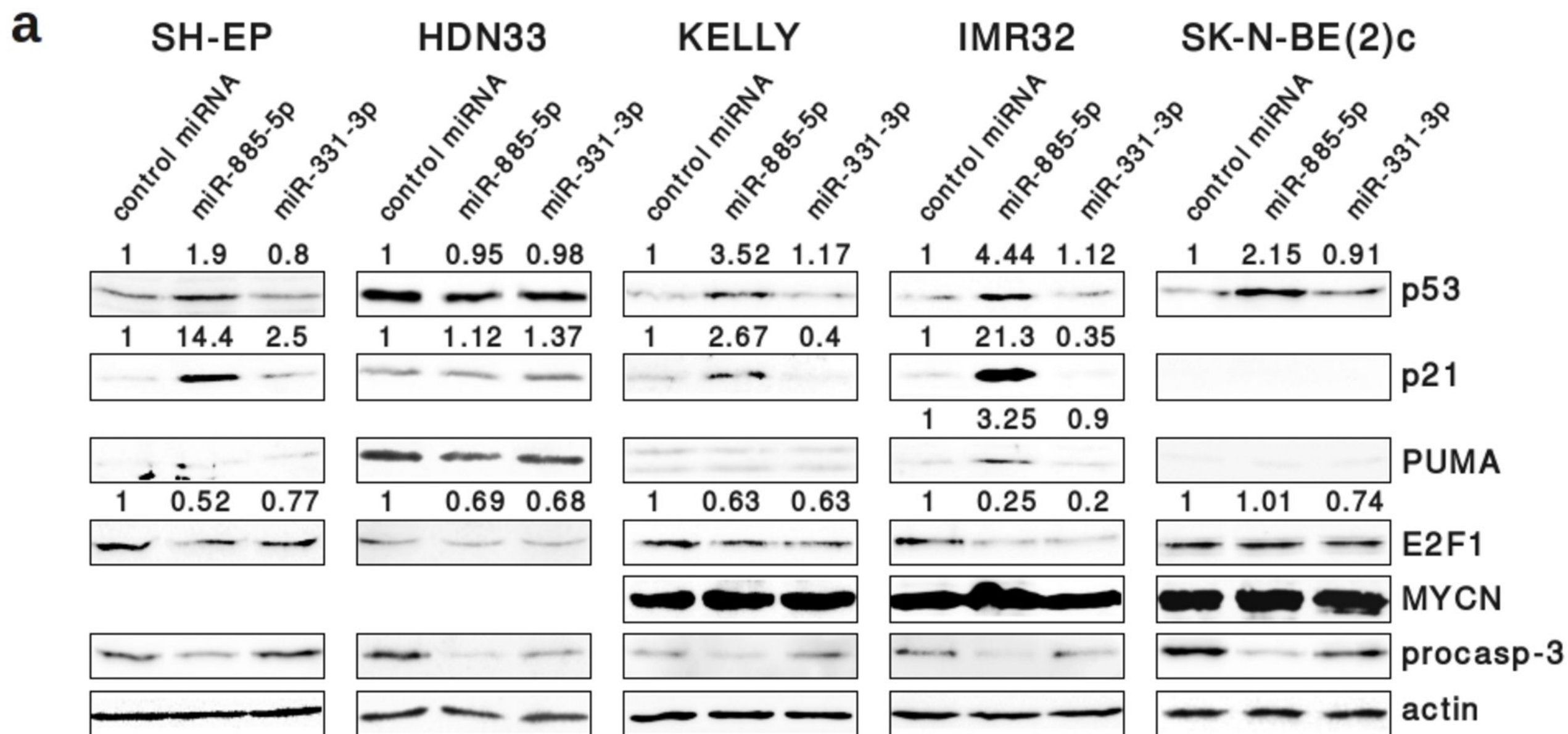
#International Neuroblastoma Staging System

b**c**

	MYCN	TP53	INK4/ARF	3p
SH-EP		wt	del	N
HDN33		mut*	del	 1 t(3;6;7;11) 1 t(3;6;11) 1 t(3;3;20) 1 t(3;20)
SH-SY-5Y		wt	del	N
SK-N-FI		mut	wt	N
MHH-NB-11	MNA	wt	wt	N
IMR32	MNA	wt	wt	N
KELLY	MNA	wt	wt	 1 normal 2 t(3;6) 1 t(3;14)
NGP	MNA	wt	wt	 1 normal 1 deleted
SK-N-BE(2)c	MNA	mut	wt	 2 normal 2 t(3;17)

d

a**b****c****d**



miR-885-5p 3' ucuccGUCCCAUCACAUUACcu 5'
 CDK2 3'UTR 5' caccuUGGGGUUUUGUAAUGac 3'

miR-885-5p 3' UCUCCGUCCCAUCACAUUACcu 5'
 MCM5 3'UTR 5' AGAGG-AAGGAGCUGUAGUGuc 3'

- pmiRGLO vector
- pmiRGLO CDK2 site
- ▨ pmiRGLO CDK2 mut site
- ▩ pmiRGLO MCM5 site
- ▤ pmiRGLO MCM5 mut site

